Available online at www.sciencedirect.com
SCIENCE DIRECT®
Organic Electronics 5 (2004) 59–65
Organic Electronics
www.elsevier.com/locate/orgel

Efficient energy transfer in organic thin films by ultra-high vacuum evaporation

W. Porzio *, U. Giovanella, C. Botta, M. Pasini, S. Destri, C. Provasi, V. Rossi

Istituto per lo Studio delle Macromolecole, ISMAC-CNR, via E. Bassini 15, I-20133 Milan, Italy

Received 23 December 2003; accepted 18 February 2004
Available online 7 March 2004

Abstract

The energy transfer in organics, aiming to optimise the performance of many LED devices, has been exploited with two suitable oligomers deposited either in multi layered or in co-evaporated films by ultra high vacuum evaporation. We have chosen two components displaying the appropriate absorption/emission windows, in fact the emission maximum of the first, a thienyl-fluorene derivative, is centred in the region where the absorption of the second, tetrahexylsexithiophene, is intense, hence guaranteeing a complete Foerster transfer even at low content of the latter. Optical microscopy investigations together with XRD analysis allowed us to get insight onto both the structure orientation and the morphology of the film components. The optical aspects of this thin layers, 15–30 nm thick, are also discussed and compared with the mono-component films obtained in the same conditions. LED prototypes were prepared and compared with analogous devices obtained by spin-coating technique. The intimate structure/morphology can readily account for the better performance of LED devices obtained by high-vacuum evaporation.

PACS: 81.15.Ef; 78.60; 73.50.M
Keywords: Film growth; Oligomer co-evaporation; Energy transfer; Photoluminescence

1. Introduction

In material science the knowledge of relationships among the structure/morphology and the pursued opto-electronic as well as photonic properties is relevant as such but achieves more importance to optimise the performance of prototypes of devices in terms of both proper choice of components and architecture and the desired region of use. In this respect organic LED preparation is exemplar [1,2].

In particular noticeable interest were devoted to the thiophene/fluorene-based molecules [3,4] due to relevant optical properties already exploited in prototypes [5–7].

The recent acquisition of organic high vacuum deposition opened the way, especially for the oligomers, to realize thin homogenous films suitable for LED devices [5,7,8].

Recently we have studied many oligomers based on thiophene and fluorene moieties with particular

* Corresponding author. Tel.: +39-02-23699371; fax: +39-02-2362946.
E-mail address: w.porzio@ismac.cnr.it (W. Porzio).

1566-1199/$ - see front matter
doi:10.1016/j.orgel.2004.02.001

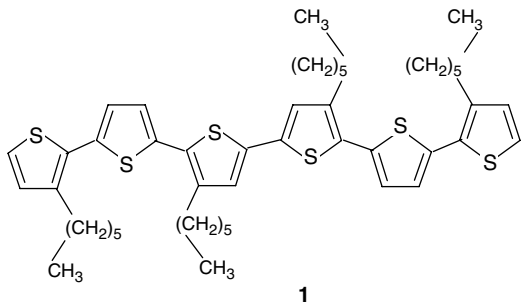

1

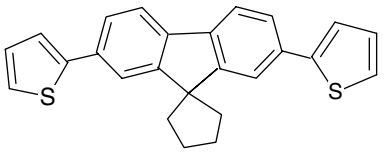

2

Scheme 1.

reference onto the relationships between solid state organization in thin films and LED-device performances [5,7,9].

One of the most drawbacks in the devices is the emission quenching due to non-radiative energy transfer among adjacent molecules or conjugated faced residues. To overcome this limit the proper blending of components, possibly at nanoscale level, have been exploited to yield promising results. Particularly when an efficient resonant energy transfer, Foerster type, between two compounds occurs [10].

We have choose the oligomers shown in Scheme 1, namely 3,3″,4‴,3⁗⁗-tetrahexyl-2,2′:5′,2″:5″,2‴:5‴,2⁗:5⁗,2⁗⁗:5⁗⁗,2⁗⁗⁗ sexithiophene (**1**) and 2,7-di(2-thienyl)-9,9-cyclopentanefluorene (**2**), which possess the appropriate photophysical properties to exploit energy transfer from **2** to **1** compounds in order to realize also LED devices based on blends of the components obtained by different techniques: casting, spin-coating and high vacuum depositions.

The structural and morphological aspects of each oligomer as well as of the blends have been related to photophysical characterizations, finally the comparison of the performances of differently prepared devices is related to these features.

2. Experimental section

The molecules above specified were prepared according to [5,11] for **1** and **2** molecules respectively. The OMBD growths were performed using the apparatus described in [12], according to the conditions reported in Table 1 for both single component growth (samples 1′–2′) and coevaporated specimen (samples 3′–4′), in the following UHV samples are referred to as thin films.

Spin coated films were obtained starting from $CHCl_3$ solutions of both molecules **1** and **2** of 8 mg cm^{-3} properly mixed to reach the molar concentrations desired (from 0.01% to 0.15% in **1**). The spinner speed was kept at 1500 rpm, at 25 °C under nitrogen flux. The corresponding drop-cast films were obtained in the same conditions. The film thickness varied according to the preparation technique, namely for spin coated and UHV films it did not exceeded 30 nm, while for cast films less than 300 nm.

The Knudsen cells used are water-flux cooled with a double filament. A slow heating ramp was properly chosen to prevent over-heating of the source. Moreover, a larger temperature at the effusion orifice with respect to the crucible base was maintained to avoid organic material re-condensation and consequently a growing stop. Basic vacuum was kept at a value less than 2×10^{-9} mbar.

Table 1
Typical UHV evaporation conditions of the molecules: Knudsen cell temperature, growth rate, thickness and molar concentration of **1** with respect **2**

Sample	Temperature (°C)		Growth rate (nm/min)	Thickness (nm)	Concentration (1 mol%)
	1	**2**			
1′	265	–	0.1	8.5	100
2′	–	187	0.9	20	0
3′	182	270	0.4	15.5	10
4′	190	248	0.7	15.5	1

XRD experiments were carried out using a computer controlled Siemens D-500 apparatus with Soller slits (2°) and narrow incident and receiving windows (0.3°). A graphite monochromator after the sample (0 0 2 direction) was inserted into a conventional Bragg–Brentano reflection geometry allowing for the observations of spacings normal or nearly normal to the substrate.

Optical microscopy observations in cross-polarized Nicol prisms were carried out using a Reichert apparatus at a maximum magnification of 400 times.

Optical microscopy observations in fluorescence mode were carried out using a Leitz Dialux apparatus at a maximum magnification of 384 times, with the conditions of light: emission 340–380 nm, cut-off filter at 430 nm and emission 450–490 nm, cut-off filter at 515 nm.

Electronic absorption spectra were recorded using a Perkin-Elmer lambda 900 instrument in transmission geometry.

CW photoluminescence spectra were carried out by using a SPEX 270M monochromator equipped with a N_2 cooled CCD detector, by exciting with a monochromated Xe lamp. Solution photoluminescence quantum yield (PLQY) measures were performed using, as a reference, a quinine sulphate solution by exciting at 350 nm ($\Phi = 54.6\%$). PLQY on films were performed using an integrated sphere and laser radiation ($\lambda = 364$ nm).

Molecular modelling calculations including crystal packing energy minimisations were performed using MATSTUDIO package, release 2.0, developed by Accelrys [13].

3. Results and discussion

The structural/morphological evidences of both molecules aiming to relate with their electroluminescence behaviour in thin films obtained by different techniques, namely ultra high vacuum (UHV) evaporation, detailed in Table 1, spin-coating and casting, have been examined by coupling the XRD analysis with fluorescence microscopy [14].

3.1. Molecule *1*

The oligomer displays polymorphism, constituted by two 3-D phases and a mesophase (smectic in nature) [14], obtained from different cooling rate from melt, namely very slow cooling (<0.01°/min) yields thermodynamically stable yellow phase (Y); while another 3D phase (R), is achievable by adopting a cooling rate of ~0.1°/min, finally the smectic phase M is prepared by liquid nitrogen quenching. The XRD patterns of films subjected to these different thermal treatments are reported in Fig. 1. However all the packing arrangements, obtained by single crystal analysis (Y-phase) [11], by powder diffraction analysis (R-phase)[15] and by crystal packing calculations (M-phase), see Section 2, allows for a bad or far facing among adjacent conjugated segments [11,15], thus limiting luminescence quenching [16]. The striking differences among the phases are the molecular conformation as shown in Fig. 2, the Y-phase presents end-thiophene rings bent by over 40° with respect to the mean molecular plane, while in the R- and M-phases the corresponding torsion angles are <10° and <20° respectively. Another characteristic difference is related to the conformation of alkyl

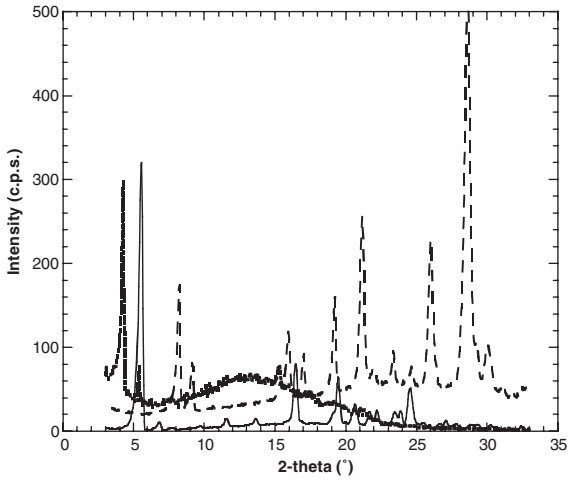

Fig. 1. XRD patterns of samples of **1** obtained by crystallization from melt at different cooling rates. The three different phases are evidenced: Y (solid line), R (dashed line) and M (dotted line), see text.

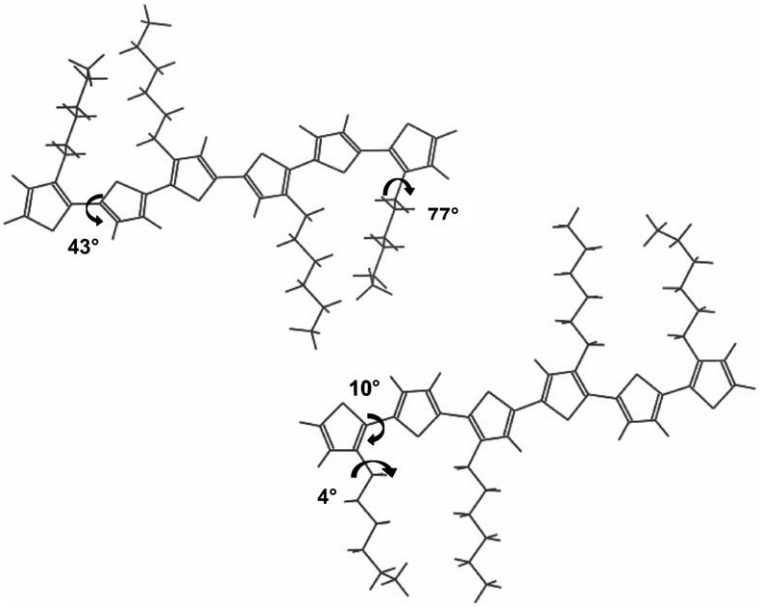

Fig. 2. Conformations of molecule **1** in the Y phase (up) and in the R- or M-phases (down).

chains which is zig-zag planar in the R- or M-phases, while assumes a tilted angle (>77°) with respect to the thiophene ring in the Y-phase; finally the terminal methyl groups assume gauche conformation in the R-phase. The UHV deposition allow for the preparation of films richer in mesophase with respect to Y-phase (~5/1 from XRD analysis) [14]; in the spin-coating films such ratio is enhanced up to ~5/1; only in films quickly cast from $CHCl_3$ the R-phase could be evidenced [14].

In Fig. 3 the absorption and emission of films Y-phase rich and M-phase rich, obtained by UHV evaporation on quartz substrates, are reported for comparison, while in Fig. 4 the normalized absorption spectra of thin films of **1** grown in UHV onto a large glass substrate, 4×2 cm^2, is shown. The reduction of the intensity (the inset of Fig. 4) together with the profile variation of the spectrum (Fig. 4) as a function of the distance between the substrate and the furnace are evident. The first observation is attributed to both the small amount deposited and mostly to the different oscillator strength. The comparison with Fig. 3 reveals different amounts of the two main phases as increasing the distance from the furnace, i.e.

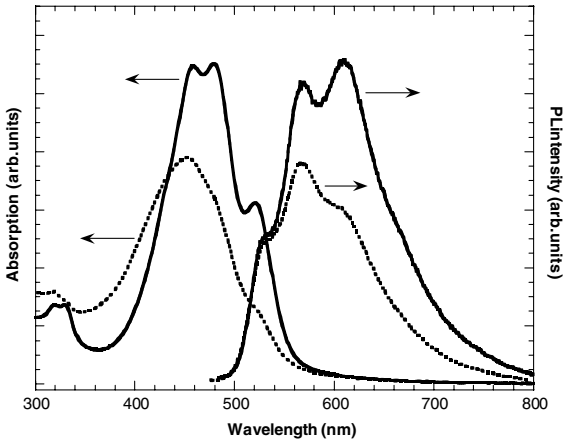

Fig. 3. Absorption (left) and emission (right) spectra of molecule **1** thin films. Y-phase (full line) and M-phase (dotted line) rich samples.

from 14 to ~17 cm. This observation is in agreement with the slightly different crystal energy, as determined by both DSC and crystal packing calculations, between the more stable the Y-phase and the M-phase, being less than 1 kcal/mol [17]. The control of the growth in these conditions, ~0.05 nm/min, consists of a delicate equilibrium

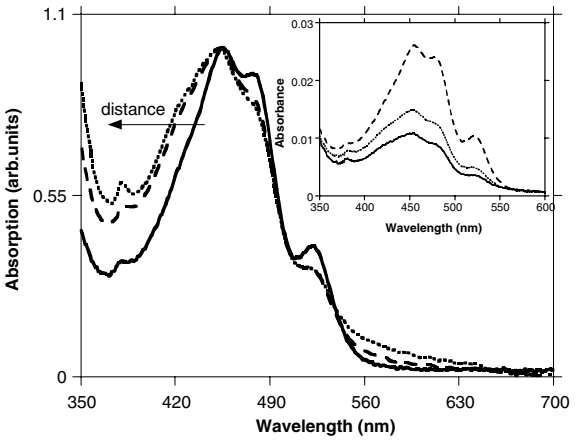

Fig. 4. Electronic absorption spectra of a thin film of **1** performed at different regions of the sample, corresponding to increasing distances from the evaporating cell. The curves are normalized while the inset ones are reported as carried out.

between the kinetic control, at a shorter distance from the furnace orifice, giving rise to M-phase rich regions, and the thermodynamic control, yielding Y-phase rich areas.

3.2. Molecule 2

The crystal of molecule **2** displays a statistical disorder at end-thiophene rings, i.e. they assume either *syn* (mainly) or *anti* conformations with respect to the central cyclopentane ring [5]. However the partial overlap of these thiophene residues allows for an energy transfer, indicated by arrows in the packing arrangement shown in Fig. 5. Films obtained by both casting and especially by spin-coating tend to crystallize/aggregate during ageing, while UHV evaporated films are more stable, although they present smaller size of crystalline domains [5]. The absorption and PL spectra of **2** thin films are reported in Fig. 6. The low-energy tail observed in PL, unshown in Fig. 6, has been attributed to aggregation of few molecules strictly π-faced [5].

3.3. Blends and devices

As also shown in Fig. 6 (UHV thin films on quartz), the absorption of molecule **1** well matches

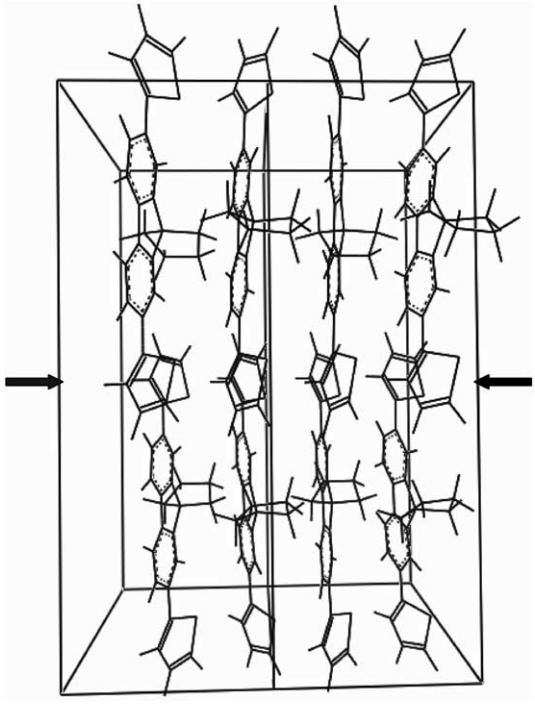

Fig. 5. Crystal packing of molecule **2**. The arrows indicate the closest pathway among conjugated segments.

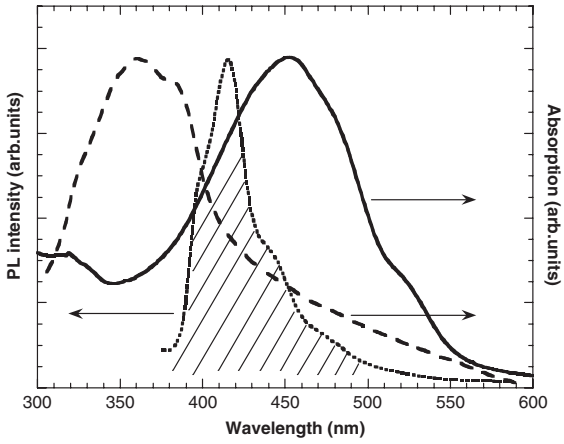

Fig. 6. Spectra of absorption of **1** (full line) and **2** molecules (broken line) and PL emission of **2** molecules (dotted line) as UHV thin films on quartz.

with the emission of molecule **2**, thus allowing a resonant energy transfer (Foerster type) to occur, evaluated according to [18]. LED devices based on

this couple of molecules display an emitting region [19] ranging from 450 to 650 nm, due to the contribution of both the compounds. The efficient energy transfer occurs in thin films, both spin-coated and UHV evaporated, even at low **1** content (less than 1%) and the Foerster radius has been calculated to be slightly lower than the experimental one 4.5 versus 5 nm, such difference has been attributed to an additional donor–donor migration [19] (see Fig. 6). The PL intensity decreases during time in spin-coated samples, with respect to UHV evaporated films, clearly due to molecule **2** crystallization.

Morphological investigations have been carried out with both optical and fluorescence microscopy, thanks to the suitable emission windows of **1** with respect to **2** thin films, allowing for an evident contrast between the dark (**2** rich) and bright (**1** rich) morphological subunits [14]. The observations revealed a decreasing segregation passing from cast, to spin-coated, to evaporated blend films [14]. Accordingly, XRD spectra show the presence of Y- and M-phases of **1** and 3-D phase of **2** molecules, the dimensions of crystalline domains of **2** molecule reduce in the series above mentioned, as clearly indicated by XRD line profile analysis [14].

LED device production was done both with spin-coated (A-type) and with UHV evaporated thin films (B-type) using the architecture ITO/PEDOT/blend/Ca/Al. The *I–L–V* curves shows a lower current density in B films with respect A ones, possibly related to reduced mobility due to crystal size dimensions, measured by line-profile XRD analysis [14]. The inset of Fig. 7 shows *I–L–V* curves of both A- and B-type devices at comparable molar ratios. The light onset depends on film thickness rather than packing effect, in fact the thickness is about 30 and 15 nm for UHV and spin coated films respectively [14].

The external efficiency is one order of magnitude smaller in device from A films with respect to B-type samples, $<10^{-4}$% and $>10^{-3}$%, respectively. This fact can be attributed to several factors: larger overall roughness in A devices; larger crystal dimensions in A device, i.e. reduced number of interfaces, and mostly crystallinity modification during the operation, relevant in A samples.

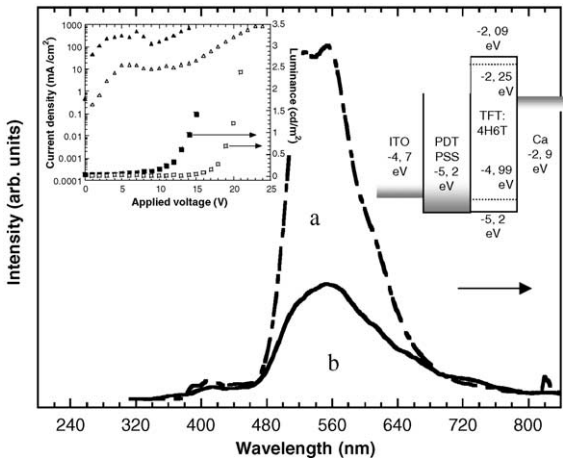

Fig. 7. PL (a) and EL (b) spectra of LED done with evaporated films 1 mol% concentrated. In the inset energy level diagram (right) of the same device and *I–L–V* curves (left) of evaporated (△, □) and spin-coated (▲, ■) devices.

4. Conclusions

A detailed study on the efficient energy transfer in thin films of two oligomers indicated:

- the relevance of the morphology of the sample, as confirmed by the efficiency in LED prototype based on blends of these oligomers;
- the efficient resonant energy transfer through blending by UHV co-evaporation;
- the different contributions in LED functioning, i.e. structural stability, segregation level, crystallite dimensions, surface homogeneity.

Acknowledgements

We thank the Italian M.I.U.R. or financial support inside the project ''Nanotechnologies''. We are indebted to Prof. A. Borghesi and Prof. A. Sassella for the experimental help in OMBD growth.

References

[1] M. Grell, D.D.C. Bradley, M. Inbasekaran, E.P. Woo, Adv. Mater. 9 (1997) 798.

[2] W. Yu, J. Pei, A.J. Heeger, Adv. Mater. 12 (2000) 828.
[3] C. Ziegler, in: H.S. Nalwa (Ed.), Handbook of Organic Conductive Molecules and Polymers, vol. 3, John Wiley & Sons, Chichester, 1997, p. 677.
[4] G. Leising, S. Tasch, W. Graupner, in: T.A. Skotheim, R.L. Elsenbaumer, J.R. Reynolds (Eds.), Handbook of Conductive Polymers, Marcel Dekker, New York, 1998, p. 847.
[5] S. Destri, M. Pasini, C. Botta, W. Porzio, F. Bertini, L. Marchiò, J. Mater. Chem. 12 (2002) 924.
[6] S. Beauprè, M. Leclerc, Adv. Funct. Mater. 12 (2002) 192.
[7] L. Antolini, E. Tedesco, G. Barbarella, L. Favaretto, G. Sotgiu, M. Zambianchi, D. Casarini, G. Gigli, R. Cingolani, J. Am. Chem. Soc. 122 (2000) 9006.
[8] S.R. Forrest, Chem. Rev. 97 (1997) 1793.
[9] S. Destri, M. Pasini, U. Giovanella, W. Porzio, Mater. Sci. Eng. 23 (2003) 291.
[10] M.A. Baldo, M.E. Thompson, S.R. Forrest, Nature 403 (2000) 750;
J. Morgado, F. Cacialli, R. Iqbal, S.C. Moratti, A.H. Holmes, G. Yahioglu, L.R. Milgrom, R.H. Friend, J. Mater. Chem. 11 (2001) 278.
[11] S. Destri, D.R. Ferro, I.A. Khotina, W. Porzio, A. Farina, Macromol. Chem. Phys. 199 (1998) 1973.
[12] R. Tubino, A. Borghesi, L. Dalla Bella, S. Destri, W. Porzio, A. Sassella, Opt. Mater. 12 (1999) 301.
[13] MATERIALS STUDIO, release 2.0, 2001, Accelrys, Parc Club Orsay Universite 20, Rue Jean Rostand, 91898 Orsay Cedex, France.
[14] W. Porzio, U. Giovanella, M. Pasini, C. Botta, S. Destri, C. Provasi, Thin Solid Films, in press.
[15] M. Neumann, C. Tedesco, S. Destri, D.R. Ferro, W. Porzio, J. Appl. Cryst. 35 (2002) 296.
[16] J. Cornil, D.A. dos Santos, X. Crispin, R. Silbey, J.L. Brédas, J. Am. Chem. Soc. 120 (1998) 1289.
[17] D.R. Ferro, W. Porzio, unpublished data.
[18] J.R. Lakowicz, Principles of Fluorescence Spectroscopy, Kluwer Academic–Plenum Publishers, New York, 1999.
[19] U. Giovanella, C. Botta, M. Pasini, W. Porzio, S. Destri, Appl. Phys. Lett. 83 (2003) 4318.